



Cite this: DOI: 10.1039/d3nr00897e

Dissociative reactions of $[\text{Au}_{25}(\text{SR})_{18}]^{-}$ at copper oxide nanoparticles and formation of aggregated nanostructures†

Jayoti Roy,^a Biswajit Mondal,^{‡a} Gaurav Vishwakarma,^a Nonappa,^b Nishanthi Vasanthi Sridharan,^{Ⓜa} Pattabiraman Krishnamurthi^a and Thalappil Pradeep^{Ⓜ*a,c}

Reactions between nanoclusters (NCs) have been studied widely in the recent past, but such processes between NCs and metal–oxide nanoparticles (NPs), belonging to two different size ranges, have not been explored earlier. For the first time, we demonstrate the spontaneous reactions between an atomically precise NC, $[\text{Au}_{25}(\text{PET})_{18}]^{-}$ (PET = 2-phenylethanethiolate), and polydispersed copper oxide nanoparticles with an average diameter of 50 nm under ambient conditions. These interparticle reactions result in the formation of alloy NCs and copper-doped NC fragments, which assemble to form nanospheres at the end of the reaction. High-resolution electrospray ionization mass spectrometry (ESI MS), transmission electron microscopy (HR-TEM), electron tomography, and X-ray photoelectron spectroscopy (XPS) studies were performed to understand the structures formed. The results from our study show that interparticle reactions can be extended to a range of chemical systems, leading to diverse alloy NCs and self-assembled colloidal superstructures.

Received 25th February 2023,

Accepted 30th March 2023

DOI: 10.1039/d3nr00897e

rsc.li/nanoscale

Introduction

Understanding chemical transformations in terms of breaking and making of bonds is the central theme of chemical science. Nanoclusters (NCs) are a unique class of nanoparticles that are gaining enormous importance due to their precise structures, specific compositions, and unique properties, similar to those of molecules. Thiolate- and alkynyl-protected atomically precise NCs of noble metals are true molecules and their science is expanding rapidly. Such NCs are $[\text{Au}_{16}(\text{SR})_{12}]^{q-}$ ($q = 4$, SR = captopril; and $q = 0$, SR = adamantanethiol), $[\text{Au}_{18}(\text{SR})_{14}]^{q-}$ ($q = 3, 4, 5$), $[\text{Ag}_{25}(\text{SR})_{18}]^{-}$, $[\text{Au}_{25}(\text{SR})_{18}]^{-/+}$, $[\text{Ag}_{29}(\text{SR})_{12}(\text{PR})_4]^{-3}$, $[\text{Au}_{38}(\text{SR})_{24}]^0$, $[\text{Ag}_{44}(\text{SR})_{30}]^{q-}$ ($q = 3, 4$),

$[\text{Ag}_{46}(\text{SR})_{24}(\text{PR})_8](\text{NO}_3)_2$, $[\text{Ag}_{40}(\text{SR})_{24}(\text{PR})_8](\text{NO}_3)_2$, $[\text{Au}_{110}(\text{SR})_{48}]^{q-}$ ($q = 2, 3$), $[\text{Au}_{110}(\text{C}\equiv\text{CR})_{48}]^{q-}$ ($q = 2, 3$), $[\text{Au}_{137}(\text{SR})_{56}]^{q+}$ ($q = 2, 3$), $[\text{Au}_{144}(\text{SR})_{60}]^{q+}$ ($q = 2, 3$), etc., where SR, PR, and $\text{C}\equiv\text{CR}$ are thiolate, phosphine, and alkynyl ligands, respectively.^{1–15} Apart from their important optical,^{13,16–19} catalytic,^{13,20–24} and luminescence^{25–32} properties and associated applications,^{33–37} they also exhibit interesting chemical phenomena. Particularly, the size- and structure-conserving chemical reactions in which core atoms undergo exchange between clusters of different kinds are important to mention.^{38,39} Interparticle reactions between these nanoparticles need to be understood in the framework of established principles of chemistry along with an atomic level understanding of the mechanisms involved. Exploration of such reactions requires precise entities such as model nanosystems mentioned earlier and molecular tools. Reactions of similar kind often have led to the creation of new molecular entities apart from simple alloy clusters. Expanding this chemistry further has resulted in tri- and tetra-metallic clusters.^{40,41}

Ligand exchange^{42–45} and metal exchange^{46,47} reactions of NCs have established that NCs can react just as molecules. $[\text{Au}_{25}(\text{SR})_{18}]^{-}$ and $[\text{Ag}_{44}(\text{SR})_{30}]^{4-}$ react spontaneously to form alloy NCs as the product.⁴⁸ Similarly, a reaction between $[\text{Au}_{25}(\text{SR})_{18}]^{-}$ and $[\text{Ag}_{25}(\text{SR})_{18}]^{-}$ was also studied in solution, where monomers and dimers of both the clusters were involved in intercluster reactions.^{49,50} Reports of interparticle

^aDST Unit of Nanoscience (DST UNS) & Thematic Unit of Excellence (TUE), Department of Chemistry, Indian Institute of Technology Madras, Chennai 600036, India

^bFaculty of Engineering and Natural Sciences, Tampere University, FI-33720 Tampere, Finland

^cInternational Centre for Clean Water, 2nd Floor, B-Block, IIT Madras Research Park, Kanagam Road, Taramani, Chennai 600113, India. E-mail: pradeep@iitm.ac.in

†Electronic supplementary information (ESI) available: Concentration calculations of the employed materials, UV-vis study, time-dependent MS studies, HRTEM micrographs, and FTIR and DLS studies. See DOI: <https://doi.org/10.1039/d3nr00897e>

‡Present address: Institute of Nanotechnology, Karlsruhe Institute of Technology, 76344 Karlsruhe, Germany.

reactions suggest that a possible route for these reactions is through the exchange of metal or metal–ligand fragments, through interparticle dimers. Monolayers of ligands protecting the surface of the NCs are dynamic, and the metal–ligand interface plays an important role in controlling the reactions.

Apart from the chemistry between clusters, cluster–bulk chemistry, for instance, the reaction of $[\text{Au}_{25}(\text{SR})_{18}]^-$ and $[\text{Au}_{38}(\text{SR})_{24}]^-$ NCs with bulk Ag–metal, has also been reported.⁵¹ This kind of exchange is elegantly seen in isotopic exchange experiments of $[\text{}^{107}\text{Ag}_{25}(\text{SR})_{18}]^-$ and $[\text{}^{109}\text{Ag}_{25}(\text{SR})_{18}]^-$ with bulk Ag–powder and related experiments.⁵² Similar atom exchange chemistry has also been seen in the reaction between clusters and metal ions, such as $[\text{Au}_{25}(\text{SR})_{18}]^-$ and Pt^{4+} , Pd^{4+} , Hg^{2+} , and Cd^{2+} leading to $[\text{MAu}_{24}(\text{SR})_{18}]^-$ (where $\text{M} = \text{Pt/Pd/Hg/Cd}$).⁹ In similar processes, the metal ions participating in the reactions get reduced by the clusters, which are charged in the native state. Recently, NCs have been used as attractive nanoscale building blocks to fabricate 3D superstructures *via* colloidal self-assembly.^{9,53,54} Exploring self-assemblies of NPs has been a hot topic in nanotechnology for the past few years and it remains relevant due to the tunable collective properties as well as the remarkable applications of the superstructures in a wide range of fields. The inter-nanocluster interactions play a vital role in the novel properties of metal nanoparticle assemblies.²² Reactions between various sized nanoparticles in homogeneous solutions constitute an emerging area in the field of NCs with great potential for the controlled formation of transition metal nanoalloys and self-assembled superstructures.⁵⁵

Multidimensional close-packed nanocluster-based molecular aggregates have been achieved using evaporation-induced assembly, interfacial assembly, binary solvent-induced assembly, the antisolvent approach, dip coating, and the Langmuir–Blodgett method.^{56–58} Still, achieving a combination of precision and reproducibility of self-assembled large-area NP superstructures remains a grand challenge. Metal NPs too exhibit polydispersity, a tendency toward uncontrolled aggregation, and a lack of directional inter-nanoparticle interactions. Additionally, rather than the anticipated homogeneous or precise product, delayed diffusion of colloidal particles and nonspecific binding may cause a variety of undesired architectures.

In this context, we decided to explore the redox chemistry between noble metal NCs, such as $[\text{M}_{25}(\text{SR})_{18}]^-$ ($\text{M} = \text{Au}, \text{Ag}$) with metal oxide and sulfide nanoparticles, such as MO_x (*e.g.*, CuO , Cu_2O , NiO , PbO , *etc.*) and Ag_2S . As this corresponds to a large chemical diversity, we decided to focus on one reaction in the present paper, namely that between $[\text{Au}_{25}(\text{SR})_{18}]^-$ and CuO NPs. These experiments suggest that chemical reactions between the systems are strongly dependent upon the concentration of the reactants. Our results suggest that simple atom exchange occurs in the low concentration limit of metal oxides. Interestingly, at a higher concentration, the clusters undergo oxidative decomposition. This results in mixed metal–thiolates, which subsequently form nanoaggregates.

Experimental section

Reagents and materials

Chloroauric acid trihydrate ($\text{HAuCl}_4 \cdot 3\text{H}_2\text{O}$), 2-phenylethane thiol (PET), tetraoctylammonium bromide (TOAB), sodium borohydride (NaBH_4), and copper acetate dihydrate $[\text{Cu}(\text{CO}_2\text{CH}_3)_2 \cdot 2\text{H}_2\text{O}]$ were procured from Sigma-Aldrich. Solvents, such as tetrahydrofuran (THF), dichloromethane (DCM), and methanol (MeOH) were purchased from Finar Limited and were of HPLC grade. Milli-Q water was used during the synthesis of NC and NP. All chemicals were utilised without further purification.

Synthesis

Synthesis of $[\text{Au}_{25}(\text{PET})_{18}]^-$. $[\text{Au}_{25}(\text{PET})_{18}]^-$ (*i.e.*, abbreviated as $[\text{Au}_{25}]$) NC was synthesized using an established literature procedure.^{59,60} About 40 mg of $\text{HAuCl}_4 \cdot \text{H}_2\text{O}$ was dissolved in 7.5 mL of THF and the solution was mixed with 65 mg of TOABr. The resulting solution was stirred for around 10–15 min to get an orange-red solution. To this solution, the PET ligand ($\sim 68 \mu\text{L}$) was added by maintaining an Au : PET molar ratio of 1 : 5 and the system was stirred continuously for another hour. The Au-thiolate complex was formed which was reduced by a solution of 39 mg of NaBH_4 in 2.5 mL ice-cold water. The color of the solution changed instantly from yellow to brown. The solution was stirred continuously for another 5 hours for the complete conversion of diverse NCs to $[\text{Au}_{25}]$. Finally, the as-synthesized cluster was vacuum dried using a rotavapor and washed several times with excess MeOH to get rid of free thiol and thiolate. Finally, the $[\text{Au}_{25}]$ NCs were extracted in acetone and the solution was centrifuged. The supernatant solution containing $[\text{Au}_{25}]$ was collected. It was vacuum dried and the residue was dissolved in DCM to prepare a stock solution. 25 μL of the stock solution ($\sim 1.35 \text{ nM}$) was used during the reaction.

Synthesis of copper oxide nanoparticles (CuO NPs). Pure metallic copper oxide nanoparticles (*i.e.*, abbreviated as CuO NPs) were prepared by the thermochemical reduction method according to a previously published method.⁶¹ In a typical synthesis, 1 g of copper acetate dihydrate was dissolved in 12.5 mL of deionized water. The solution was stirred for one hour until the salt was dissolved completely. The resulting reaction mixture was heated in a muffle furnace at 500 °C for one hour under atmospheric conditions. A dark blackish-brown precipitate was formed after one hour. The reaction mixture was cooled at room temperature and washed with a 2 : 3 MeOH–water solution. Finally, the CuO NPs were washed with MeOH. The pure bare CuO NPs were dried under 60 °C for 30 minutes. 1 mg of the as-synthesized NPs was dispersed in 1 mL of DCM to prepare the dispersed solution of 1 mg mL^{-1} .

Instrumentation

UV-vis studies were performed using a PerkinElmer Lambda 25 UV-vis spectrometer in the range of 1100–200 nm at a scan rate of 240 nm per minute. All ESI MS studies were performed

in the negative ion mode using a Waters Synapt G2-Si high-definition mass spectrometer (HDMS). During measurements, capillary voltage, cone voltage, and source offset were maintained at 3 kV, 120–150 V and 80–120 V, respectively to obtain well-resolved mass spectra. The source temperature and desolvation temperature were maintained at 100 and 150 °C, respectively. The desolvation gas flow was maintained at 450 L h⁻¹ during the measurements. ESI MS, in a time-dependent manner, was employed to study the progress of the reaction between NPs and NC. 1 mL solution was taken out from the reaction vessel each time and centrifuged at 10 000 revolutions per minute (rpm) for complete removal of bigger particles and aggregates. TEM images of the samples were obtained with a JEOL 3010 instrument at an operating voltage of 200 kV with an ultrahigh resolution (UHR) polepiece. 3 μL of each sample solution was drop cast over a TEM grid (specifically carbon-coated Ni grid) and dried under an ambient atmosphere before imaging. The 2D projections for electron tomography were collected using transmission electron microscopy (TEM) operating at an accelerating voltage of 300 kV on a JEOL 3200FSC. Image acquisition was done using SerialEM software. A Malvern Zetasizer Nano ZSP instrument was utilized to study particle size distributions in solution, using dynamic light scattering (DLS). The XPS measurements were performed using an ESCA Probe TPD spectrometer of Omicron Nanotechnology. Polychromatic Al K α was used as the X-ray source ($h\nu = 1486.6$ eV). After the reaction, the NPs were directly drop cast on the sample stub. A constant analyzer energy of 20 eV was used for the measurements. Binding energy (BE) was calibrated with C 1s at 284.8 eV. All the XPS spectra were deconvoluted using the Casa XPS software. Fourier transform infrared (FTIR) spectra were measured with a PerkinElmer Spectrum 2 spectrometer with a UATR attachment. Each spectrum was collected in the wavenumber range of 400–4000 cm⁻¹.

Results and discussion

Characterization of the starting materials

Bare CuO NPs and [Au₂₅] NCs were initially selected as model systems to explore the interparticle reaction between CuO NPs and atomically precise gold NCs because of their excellent stability individually. Atomic precision of [Au₂₅] NCs was confirmed by UV-vis and ESI MS measurements. The characteristic peaks of [Au₂₅] NCs at 675 nm and 450 nm were observed in the UV-vis spectrum (Fig. S1†). Negative ion mode ESI MS measurements showed the monoanionic molecular ion peak of [Au₂₅] at m/z 7393 (Fig. S2†). The experimental isotopic distribution of the nanocluster composition of [Au₂₅] is in good agreement with the calculated one, as shown in Fig. S2.†

TEM micrographs of the as-synthesized [Au₂₅] NC are shown in Fig. S3(A(i and ii)).† A honeycomb-like arrangement consisting of NCs was observed under the electron microscope. The observed morphology of NCs could be due to the interactions among PET ligands during the evaporation of the

solvent.^{53,62,63} The CuO NPs were synthesized using the protocol discussed in the Experimental section. The TEM micrographs of the as-synthesized CuO NPs are shown in Fig. S3(B(i)).† An inter-planar distance of 0.27 nm and the EDS elemental composition further confirm the formation of CuO NPs (Fig. S3(B)).†^{61,64}

Reaction between CuO NPs and [Au₂₅] NCs

The reaction between CuO NPs and the [Au₂₅] NCs was demonstrated by mixing a known volume of DCM solution of [Au₂₅] and a dispersion of CuO NPs, also in DCM, at fixed concentrations (w/v) under stirring conditions (see the Experimental section and the ESI†). Molecular changes in the cluster were confirmed by UV-vis spectroscopy (Fig. S1†) by separating the NCs from NPs using high speed centrifugation of the solution. The red shift in the absorbance peaks of Au₂₅ after the reaction with NPs may be attributed to the exchange of surface atoms with Cu (see Fig. S1†) and the process seems to attain rapid thermodynamic equilibrium. Cu (1.28 Å) has a smaller atomic radius than gold (1.44 Å), and the Cu–Au bond (bond dissociation energy, EBD = 227.1 ± 1.2 kJ mol⁻¹) is slightly stronger than the Au–Au bond (EBD = 226.2 ± 0.5 kJ mol⁻¹).⁶⁵ Thus, Cu doping to [Au₂₅] NCs is possible and it significantly alters the optical properties of the parent NC. Relative lower energy shift in the optical absorption spectrum (as shown in the inset of Fig. S1†) can be attributed to the reduction in the HOMO–LUMO gap of the parent NC due to the formation of Cu-doped NCs. This also indicated that all or most of the Cu-doped NCs are expected to have a core–shell structure.⁶⁶ Experimental studies of the NC and NP reactions revealed that coinage metal doping alters the optical properties and oxidation states of the NC in solution.

We attempted to understand the chemical changes during the reaction using time-dependent mass spectrometric studies. To monitor the progress of the reaction, the reaction mixture was analysed after a certain time interval with ESI MS measurements. As described in the Experimental section, after a constant time interval ($\Delta t = 30$ min), the solution was centrifuged and the blackish brown supernatant was subjected to mass spectrometric studies. All the mass spectrometric parameters were kept constant throughout the experiment to analyse the compositional variation of the reaction mixture with time. As shown in Fig. 1(A) and Fig. S4, S5,† a peak of monoanionic [Au₂₄Cu₁(PET)₁₈]⁻ (m/z 7260) (the difference in mass from the parent [Au₂₅], Δm , is = 131 = [m_{Au} - m_{Cu}] = [196.9 - 63.5]) (abbreviated as [Au₂₄Cu₁]), [Au₂₃Cu₂(PET)₁₈]⁻ (m/z 7129) (abbreviated as [Au₂₃Cu₂]) (here, $\Delta m = 262 = [m_{\text{Au}} - 2m_{\text{Cu}}]$) along with a few other peaks (m/z 2100–5000) corresponding to other intermediate species appeared with time. Fluctuating intensity trends of [Au₂₄Cu₁] and [Au₂₃Cu₂] were observed during the course of the reaction (Fig. 1(A)(a–d and a'–d')). The parent [Au₂₅] NC (m/z 7393) showed a continuous reduction in the signal intensity during the reaction (peak at m/z 7393 in Fig. 1(A(i–v))). The exact number of copper atoms doping into the gold NC was confirmed from the exact matching of experimental isotopic distribution with the calculated

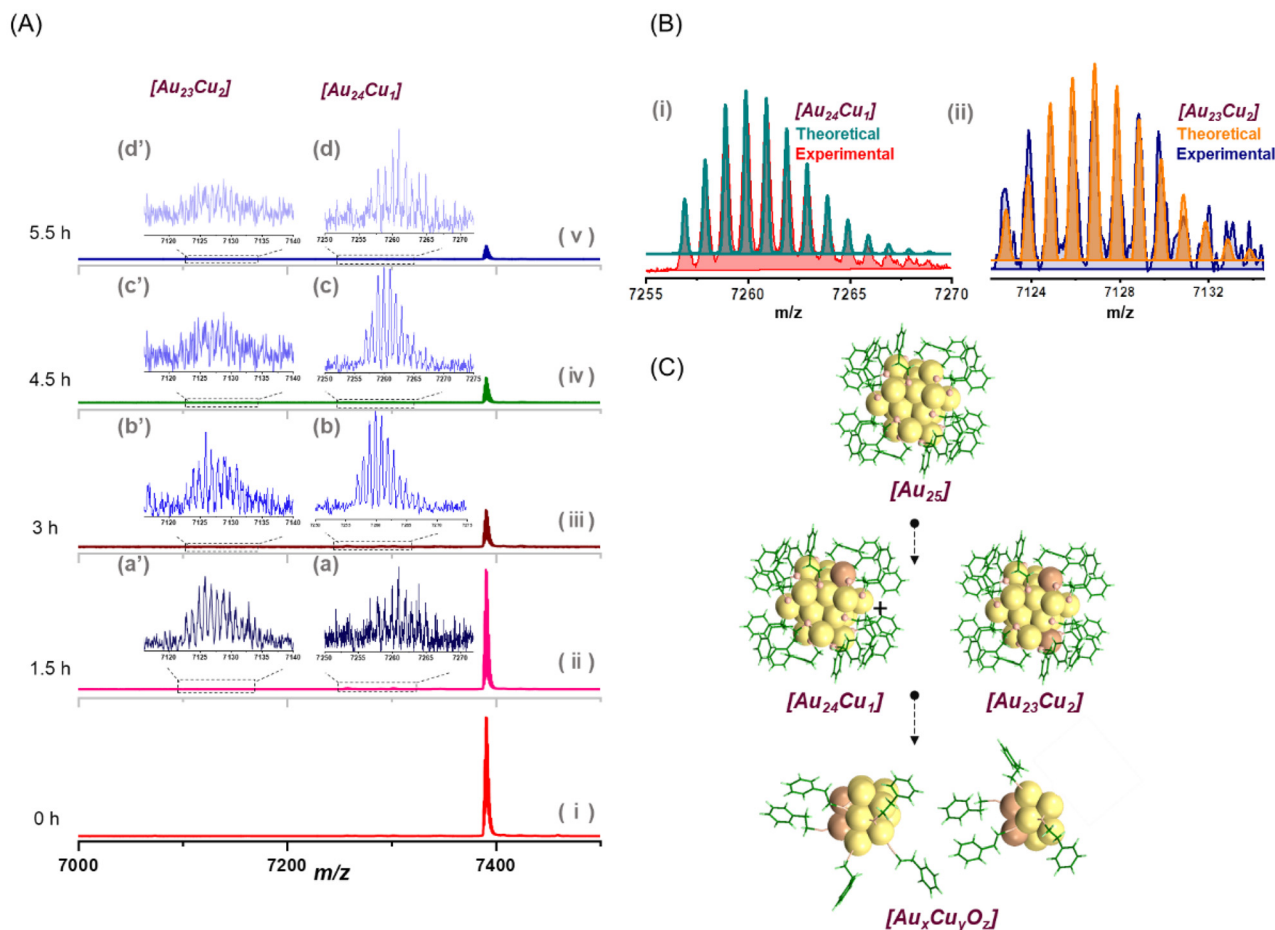


Fig. 1 (A(i–v)) Time-dependent ESI MS spectra of the NC solution in the mass range of m/z 7000–7500. During the reaction, the time-dependent evolution of copper-doped NC species, [Au₂₄Cu₁] and [Au₂₃Cu₂] are observed in the mass spectral region of m/z 7250–7272 (a–d) and m/z 7116–7140 (a'–d'), respectively. (B) High-resolution isotopic distribution of the mass spectrum of [Au₂₄Cu₁] (i) and [Au₂₃Cu₂] (ii) with their calculated ones (green and orange, respectively). The experimental mass spectra in (B) were obtained from the 3 h-spectral data (1(A)(iii)) to fit with the theoretical ones. (C) Schematic representation of the reaction at [Au₂₅] NCs in the course of time.

mass spectrum (as shown in Fig. 1(B)(i and ii)). The experimental mass spectra of the specific m/z range in Fig. 1(B) were recorded from the MS data after 3 h of reaction (Fig. 1(A)(iii)) to fit with the respective theoretically calculated mass. The variation of ion abundances of copper-doped [Au₂₅] NCs can be correlated with the formation of other intermediates in the m/z range of 2100–5000. The time-dependent ion intensity variation of [Au₂₄Cu₁] and [Au₂₃Cu₂] NCs is shown in Fig. S4(B).† The formation of monoanionic metal-thiolate intermediates, such as [Au₈(PET)₉][−] (m/z 2820), [Au₈(PET)₁₂O₂][−] (m/z 3256), [Au₁₀(PET)₁₀O₂][−] (m/z 3378), [Au₁₀(PET)₁₀][−] (m/z 3396), [Au₉Cu₂(PET)₁₁][−] (m/z 3411), and [Au₁₁(PET)₁₀(O₂)₂][−] (m/z 3601) was seen in the course of reaction (see Fig. S5 and S6†). As we did not observe any NC fragments containing O or O₃, such fragments can also be attributed to S or S₂ instead of O₂ and (O₂)₂ addition. It is difficult to differentiate one such NC fragment containing O₂ instead of S (O₂ and S have the same mass) by looking into the high-resolution isotopic distribution. So, the molecular compositions with O₂ can be varied

with S. Moreover, it has been reported that after losing all 'staple' Au-PET units, [Au₂₅] NC forms Au_xS_y fragment ions during its gas-phase fragmentation.¹⁵ When the NCs were accommodated on the surface of CuO NPs during the reaction, atomic exchanges took place between the NPs and the NCs. As a result of this interparticle interaction between NCs and NPs, Cu-doped [Au₂₅] and other Cu and O-doped smaller Au-NC fragments were formed. Because of the accessible sites of [Au₂₅] NC,⁶⁷ Cu and O atoms of NPs can interact with Au-S staples on the surface of the NC. The interactions between Cu- and O-atoms of CuO NPs with the [Au₂₅] NC during the solution phase reaction resulted in the decomposition of the parent [Au₂₅] NC.⁶⁸

These reactions are found to be highly dependent on the concentration (w/v) of the dispersed solution of CuO NPs. Lower the concentration of the NPs, the slower is the kinetics of the reaction. For example, for a very low concentration of CuO NPs (1/5th (w/v) of the prepared stock solution), only singly copper-doped [Au₂₅] NCs were formed (see Fig. S7†).

The thiolate fragments indicated that the process may lead to the assembly of small clusters, mediated by thiolates. We find that all the fragments, including the alloy NCs formed during the reaction, finally coalesce to form nano-assemblies, as observed in TEM images (see Fig. 2). In Fig. 2, we observed that the size of the parent CuO NPs decreases from ~ 50 nm to < 10 nm during the interparticle reaction with $[\text{Au}_{25}]$ NCs (also see Fig. S8†). The bare parent CuO NPs tend to be intermingled with the NCs, as shown in Fig. S8(A)†. In Fig. 2(B), TEM images showed the formation of three-dimensional nanosphere (NS)-shaped assemblies after six hours of reaction. At this stage of the reaction, the size of homogeneous NSs was expanded to a diameter regime of 200–400 nm. Large area TEM (Fig. 2(B)) and scanning transmission electron microscopy (STEM) (Fig. S9(A)†) micrographs showed the formation of well-shaped NSs.

Differential centrifugation was performed to separate the self-assembled superstructures, *i.e.*, NSs from parent NPs and NCs. Initially, NPs were separated from the rest of the solution; later, NSs were precipitated out from the solution. Elemental compositions of the NPs, NSs, and NCs were analyzed by EDS (Fig. S10–S13†). Fig. S11 and S12† show the TEM micrographs of isolated NSs (as the precipitate) and reacted NCs (as the supernatant) after centrifuging the reaction mixture at 9000 rpm. The precipitate (see Fig. 3(A(i–v))) and supernatant (see Fig. 3(B(i–v))) obtained after centrifugation were used for STEM and EDS elemental mapping.

EDS mapping confirmed the presence of gold, copper, sulfur, and oxygen as elemental composition in the structures (Fig. 3(A(ii–v))). It is important to note that as shown in Fig. 3(B(ii–v)), gold, copper and sulfur are present throughout the NC aggregates, suggesting that the copper was doped into the NC. The elemental maps suggest that oxygen is concentrated in the nanospheres and not in the NC aggregates. This would mean that NCs are doped predominantly with Cu and no additional chemical changes have occurred. However, in the

CuO particles, the incorporation of Au and S has occurred. As the only source of S is NCs, they have undergone partial degradation.

To gain insights into the morphology of assembled nanostructures, and thus to have a better understanding of the assembly of NC–NP fragments, TEM tomographic reconstruction was performed. Fig. 3(C(i–iii)) shows the TEM micrographs at three different tilt angles. For 3D reconstruction of the structure, a series of 2D projections were collected by tilting the sample from $+69^\circ$ to -69° with an increment angle of 2° . 3D reconstruction suggests sphere-like assembly. It must be noted that due to possible drying effects, the spherical superstructures were partially deformed (Fig. 3D, see ESI Video V1† for tilt series of aligned 2D projections). The 3D reconstructed image and the cross-sectional view suggest densely packed nanoparticles throughout the spherical superstructure with slight differences in the core and peripheral regions (Fig. 3D, see ESI Video V2† for 3D reconstruction of the nanosphere). Importantly, nanoparticles were distributed throughout the sphere, though without a regular order or packing pattern.

To examine the changes in the chemical environment upon reaction between NPs and NCs, an XPS study was performed. XPS revealed a change in the oxidation state of elements as a result of the reaction. In Fig. 4, the Au 4f region shows a blue shift in the binding energy (BE) corresponding to the oxidation of Au (due to Au–Cu bond) upon reaction with CuO NPs. The Cu $2p_{3/2}$ peak of reacted CuO was shifted to lower BE after the reaction, due to the reduction of a fraction of Cu(II) to Cu(I). Additionally, reduction in the strong satellite peaks corresponding to Cu(II) (prominent in parent NPs), can be noticed after the reaction. These observations suggest a mixed oxidation state of Cu after the reaction.

Similarly, S 2p BEs were compared before and after the reaction. The peak at 162 eV corresponds to $2p_{3/2}$ of S, attributed to the Au–S bonds. The appearance of a new peak at 167.2 eV

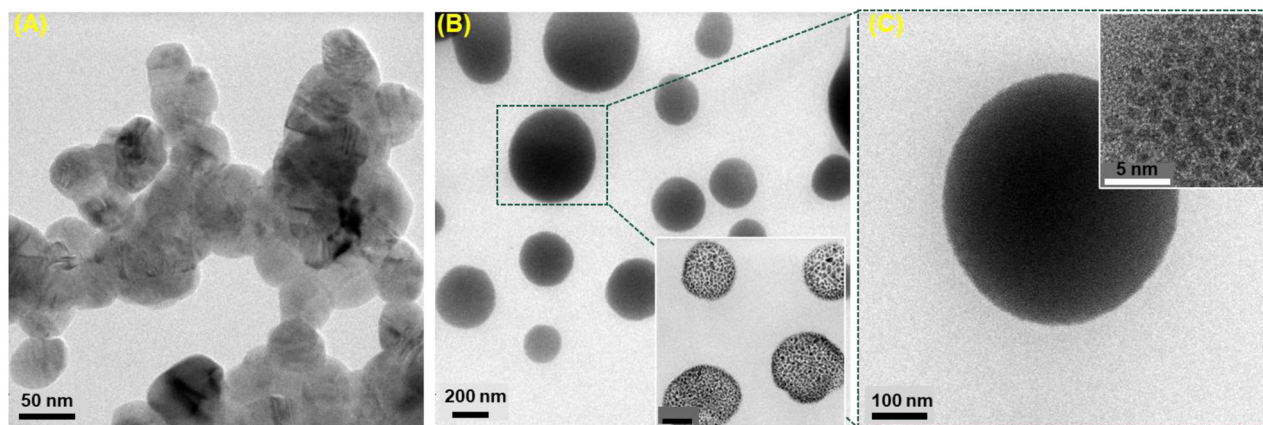


Fig. 2 TEM images (left to right) showing bare CuO NPs before (A) and after (B) reaction with Au_{25} NCs. CuO NPs with an average size of ~ 50 nm (A) and assembly formed post reaction (B). A second kind of assembly was observed in the inset of (B). Other than NSs, unreacted and reacted NPs were observed under TEM which are presented in the ESI.† In (C), higher magnification TEM image of a single nanosphere. Inset shows the HR-TEM from a selected area.

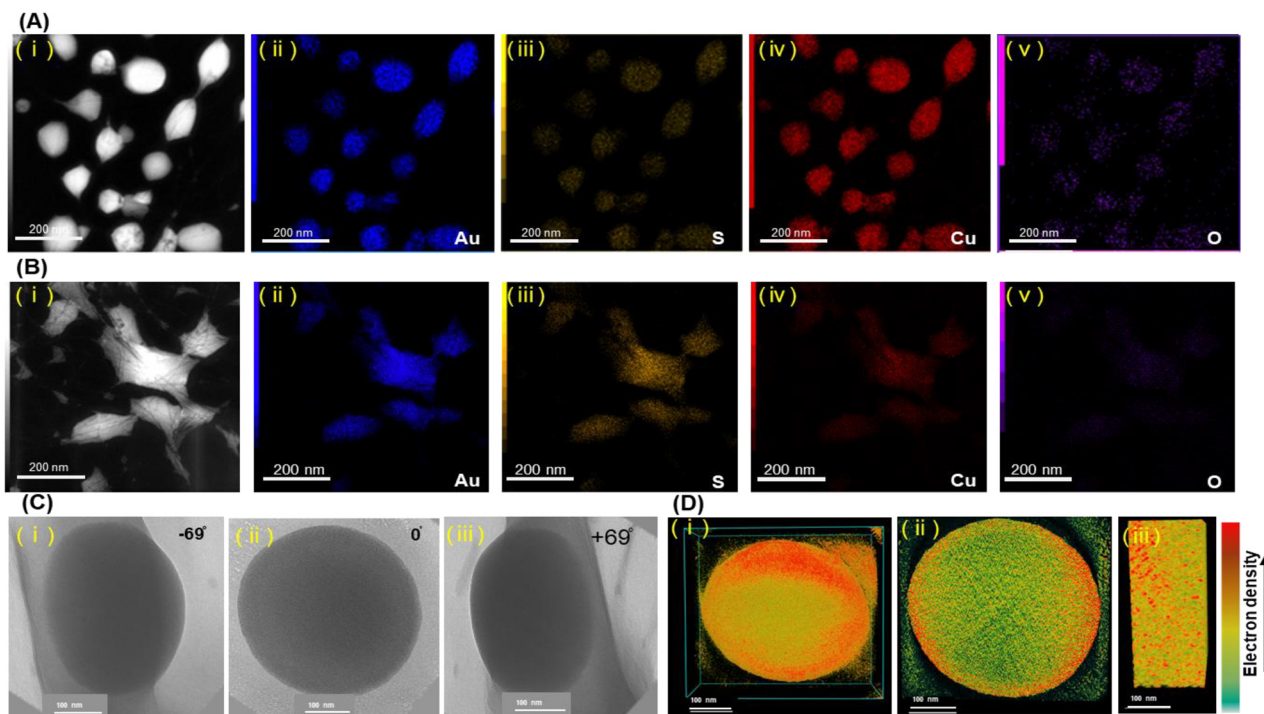


Fig. 3 (A and B) DF STEM images of nanosphere and reacted nanoclusters, respectively and corresponding EDS elemental mapping for Au, S, Cu and O. (C) 2D TEM projection of a spherical superstructure at different tilt angles. (D) TEM tomographic reconstruction of C, cross-sectional view, and a portion showing densely packed nanoparticles.

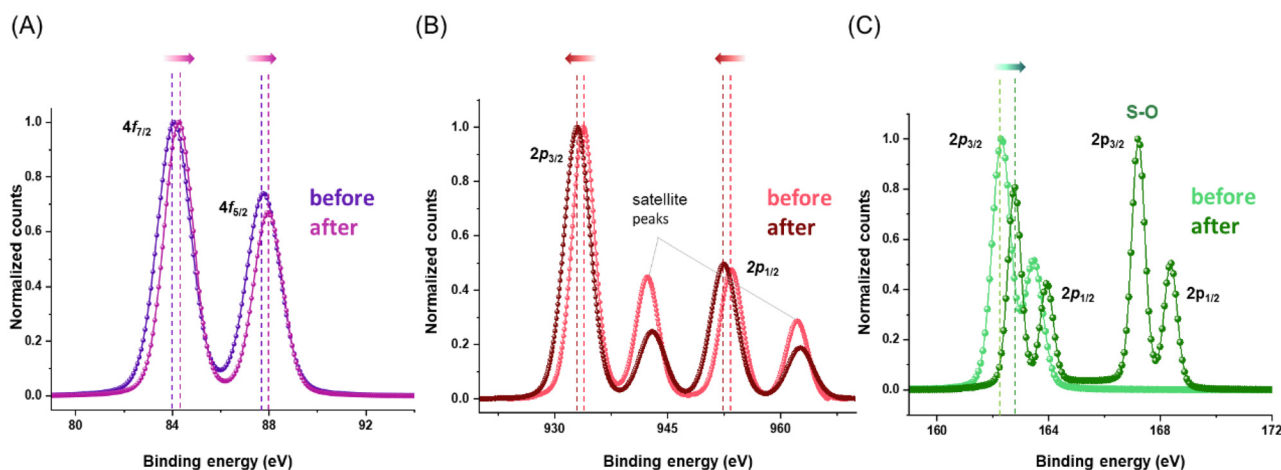


Fig. 4 XPS spectra of (A) Au 4f, (B) Cu 2p, and (C) S 2p regions, before and after the reaction.

in the XPS study of reacted NPs indicates the formation of a new S–O bond as a result of the reaction of NPs with NC. So, it is revealed that strong electrostatic and coordination interactions between Au–S of NCs and Cu–O atoms of NPs enhance the NC–NP interactions and atomic exchange during the reaction.

To understand the molecular interactions responsible for the formation of nanoaggregates after the reaction, FTIR measurements of the supernatant (see Fig. S14(ii)†) after reac-

tion were carried out. The resultant FTIR data were compared with $[\text{Au}_{2.5}]$ NC (Fig. S14(i)), TOAB (Fig. S14(iii)), and PET (Fig. S14(iv)).† New IR frequencies (ν) were observed due to new C–O and S–O bonds and also due to intermolecular hydrogen bonding (H-bonding) as a result of the reaction. The spectra are shown in Fig. S14.† In Fig. S14,† the progression bands in the range of $1900\text{--}1700\text{ cm}^{-1}$ in $[\text{Au}_{2.5}]$ vanished completely after the reaction, indicating the loss of crystallinity and degradation of NC during the course of the reaction. The

formation of C–O and S–O bonds indicate atom transfer between precursors during the reaction. As a corollary, these non-covalent and covalent interactions play a vital role in the formation of molecular nanoaggregates and NSs.

DLS has been utilized to reveal the size evolution of nanostructures in solution as a function of reaction time. Time-dependent DLS measurements (see Fig. 5) of the reaction showed a gradual increment in the hydrodynamic radius (R_H) of the NSs after 2 h of the reaction. Additionally, DLS measurements revealed that the average radius of the NS aggregates gradually increased between 2 to 5 h continuously. Furthermore, the average R_H of NSs remained constant (*i.e.*, average R_H during 5 h of the reaction) with a further increase in the reaction time (~ 6 h). Hence, this proves the formation of NSs in the solution phase with excellent colloidal stability.

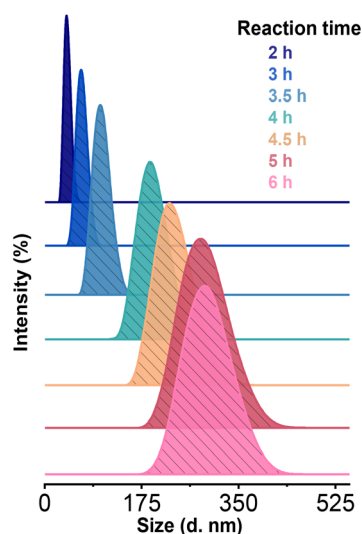
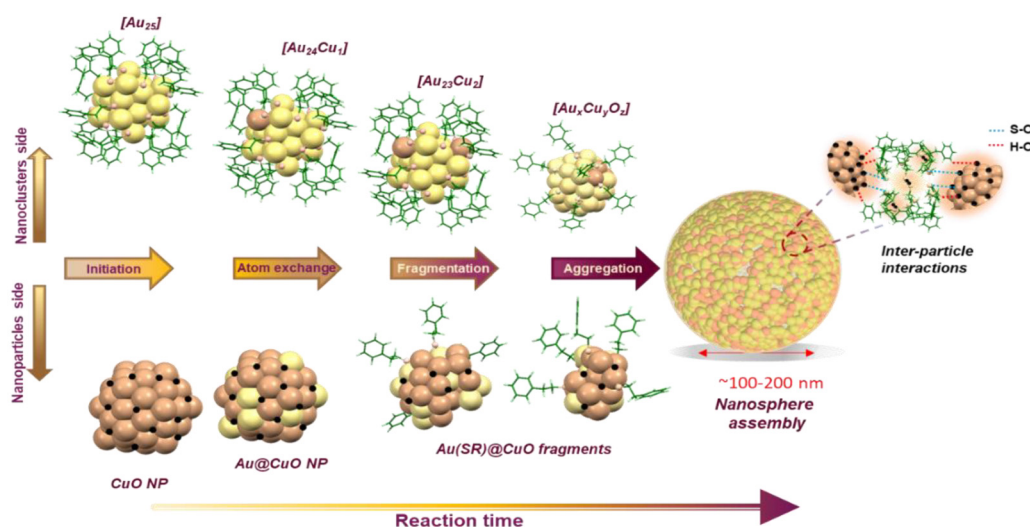


Fig. 5 Time-dependent monitoring of the reaction by DLS.

A similar DLS experiment was demonstrated to probe into the disassembly of nanoaggregates (see Fig. S15[†]). Solvent plays an important role in growth of nanoparticles, their assembly, and disassembly. Interactions between the nanoparticle surface and solvent molecules or between the solvent molecules and ligands considerably influence the particle size and morphology. Methanol was gradually added to the reaction medium (*i.e.*, DCM solution) at the end (after six hours) of the reaction, and DLS was performed. In a highly polar dispersion medium, charged thiolate complex ions (which were earlier assembled to form NSs) are more soluble. As a result, particles are prevented from aggregation, and disassembly of NSs was observed. As shown in Fig. S15[†], the average R_H of NSs was ~ 301 nm after 6 h of reaction. However, after 10 μ l of MeOH addition, R_H increased. But, with further increment in MeOH (50–100 μ l), the R_H started decreasing. More disaggregation was observed by introducing more (~ 250 –500 μ l) MeOH to the reaction mixture. As a result, the peak at ~ 300 nm decreased while an intense new peak at ~ 98 nm, appeared (see Fig. S15[†]). The disassembly of NS after the addition of MeOH was further confirmed by TEM imaging (Fig. S16[†]).

Mechanism of formation of NSs

We suggest that the polymerization of Cu-doped Au-NC fragments with the smaller-sized alloy-NP fragments *via* direct assembly leads to the formation of supramolecular architectures. During the initial stage of this process, along with the generation of smaller thiolate-protected copper-doped gold NCs, smaller NPs were also formed, which, in turn, arranged systematically due to the covalent and non-covalent interactions leading to the spherical entity in the final stage (see Scheme 1). This self-assembly is mainly driven by hydrogen bonding, van der Waals interactions, C–H \cdots π / π – π interactions,⁶⁹ metallophilic (as seen in Fig. 1–3) and covalent bonding (*i.e.*, S–O, C–O) (as noticed in Fig. 4 and Fig. S14[†]), and amphiphilic interactions (as observed in Fig. 5, and



Scheme 1 Structural evolution of nanosphere formation during the reaction between NC and NP.

Fig. S15†) between the NP and NC fragments. These interactions within NP assemblies may produce novel properties, such as efficient charge transport, enhanced conductivity, *etc.*, due to the synergistic effects between thiolated NP fragments. Also, shape complementarity of ligands on reacted particle fragments could be responsible for the strong attractive forces to form the nanoassembly.

Based on the spectrometric, microscopic, and spectroscopic investigations, we propose that the formation of the vesicle-like nano-assembly during interparticle reactions relies on the following aspects: (i) formation of S–O and C–O bonds between surface ligands of reacted NCs and CuO NPs (see Fig. S14(ii)†); (ii) the $\text{CH}\cdots\pi/\pi\cdots\pi$ and $\text{H}\cdots\text{H}$ interactions between thiolates of doped NPs and NCs and (iii) polymerization of Cu-doped NC and NP fragments. The overall mechanistic pathway of the reaction between CuO NPs and $[\text{Au}_{25}]$ NCs is shown in Scheme 2. The mechanistic pathway to form aggregated nanostructures consists of two steps. In the initial step of the reaction (*i.e.*, path A of Scheme 2), atomic exchange and redox reaction take place between NCs and NPs. Negishi *et al.* have studied the effect of Cu-doping on the electronic structure, geometric structure, and stability of Au_{25} in detail.⁶⁶ Most likely, in a single Cu-doped Au_{25} nanocluster, preferentially, a Cu atom occupies the center of the Au_{13} metal core due to the smaller atomic radius of Cu (1.28 Å) than gold (1.44 Å). The second Cu atom in the $\text{Cu}_2\text{Au}_{23}$ nanocluster can exist on the icosahedral surface or the staple position.⁶⁶ As per our XPS study, we understood that during the chemical reaction, a fraction of Au atoms underwent oxidation. In contrast, reduction occurred for some Cu atoms of the nanoparticles. The core Au atom of Au_{25} may be removed as Au^{1+} , and Cu^{2+} gets reduced to Cu^0 and occupy the central position of the nanocluster. Moreover, doping processes enhanced the formation of Cu and O-doped NC fragments and Au-thiolate doped NP fragments as noticed in the ESI MS study. The doped fragments of NC and NPs coalesced together to produce NS-like assemblies in the final step (*i.e.*, step B of Scheme 2) of the reaction.

The NC-based assembly plays a key role in customizing advanced functional materials *via* collective and synergetic properties between neighboring building blocks. It is crucial to develop a workflow to witness interparticle interaction-driven self-assemblies between NCs and NPs in the sub-nano-

meter regime to understand the chemistry of heterometallic superstructures. Moreover, recent achievements in interparticle interaction also manifest in the controlled formation of various superstructures, such as NC-mediated precision nanowire assemblies, NP-templated cluster assemblies or superlattice arrangement.^{57,70,71} The chemistry presented here suggests that the NC behaves similarly to molecules. It was demonstrated that NCs undergo oxidation, reduction (observed in UV-vis, XPS studies), decomposition (indicated in MS-based studies), and aggregation (noticed in TEM, and STEM micrographs), similar to the molecular systems. The redox chemistry occurs between systems with largely varying dimensions from 1 nm to 100 nm leading to aggregated structures of micrometer dimensions. This controlled chemical evolution from chemical reaction between clusters and NPs may be useful in making complex architectures. Such nanostructures composed of multiple metal ions with mixed properties may become useful in applications such as catalysis and magnetism.

Conclusions

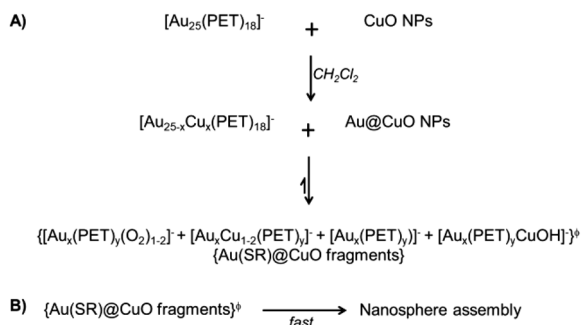
Polydispersed CuO NPs and PET-protected $[\text{Au}_{25}]$ NCs were used in our study to explore the consequence of possible atom transfer processes between NCs and NPs. Upon increasing the concentration of the oxide NPs, sphere-shaped nanoaggregates were formed along with Cu-doped NCs. The atom exchange rate enhanced the formation of smaller PET-protected multi-metallic cluster fragments which eventually coalesce to form macro-scale spherical aggregates. We monitored the reaction in a time-dependent fashion. The NSs formed were disassembled with increasing solvent polarity. Our study demonstrates the spontaneity of atom transfer when NCs are brought in contact with metal-oxide NPs. Such NC–NP reactions can provide an entirely new method of generating multimetallic and uniform complex architectures. This method may be extended to other metal-chalcogenide systems such as CuS, CuSe and CuTe and oxides such as MnO, ZnO, and NiO to expand the properties of the products.

Author contributions

T. P. proposed the project. J. R. performed the experiments. J. R. performed mass spectrometric, UV-vis, and DLS measurements. J. R. and B. M. carried out TEM studies. J. R. and G. V. carried out XPS studies. J. R., N. V. S., and P. K., prepared the samples. N. performed STEM imaging, EDS analysis, and electron tomography reconstruction. J. R. wrote the first draft of the manuscript, and the final version of the manuscript was prepared through the contributions of all authors. All authors have given approval to the final version of the manuscript.

Conflicts of interest

There are no conflicts to declare.



Scheme 2 Mechanistic pathway of the reaction.

Acknowledgements

We thank the Department of Science and Technology, Government of India, for supporting our research programme. J. R. and G. V. thank IIT Madras for the doctoral research fellowships. B. M. thanks IIT Madras for the postdoctoral fellowship. N. V. S. thanks the Pradeep Research Group for a summer project opportunity. T. P. acknowledges funding from the Centre of Excellence on Molecular Materials and Functions under the Institution of Eminence scheme of IIT Madras. N. acknowledges the Academy of Finland project funding (no. 352900), the Photonics Research and Innovation (PREIN) flagship and facilities at the OtaNano-Nanomicroscopy Center (Aalto-NMC).

References

- Q. Yao, X. Yuan, V. Fung, Y. Yu, D. T. Leong, D. E. Jiang and J. Xie, *Nat. Commun.*, 2017, **8**, 1–11.
- S. Gaur, J. T. Miller, D. Stellwagen, A. Sanampudi, C. S. S. R. Kumar and J. J. Spivey, *Phys. Chem. Chem. Phys.*, 2012, **14**, 1627–1634.
- Y. Negishi, K. Nobusada and T. Tsukuda, *J. Am. Chem. Soc.*, 2005, **127**, 5261–5270.
- X. Kang, H. Chong and M. Zhu, *Nanoscale*, 2018, **10**, 10758.
- C. P. Joshi, M. S. Bootharaju, M. J. Alhilaly and O. M. Bakr, *J. Am. Chem. Soc.*, 2015, **137**, 11578–11581.
- L. G. AbdulHalim, M. S. Bootharaju, Q. Tang, S. Del Gobbo, R. G. AbdulHalim, M. Eddaoudi, D. Jiang, O. M. Bakr, L. G. AbdulHalim, M. S. Bootharaju, Q. Tang, S. Del Gobbo, R. G. AbdulHalim, M. Eddaoudi, D. Jiang and O. M. Bakr, *J. Am. Chem. Soc.*, 2015, **137**, 11970–11975.
- M. Bodiuzzaman, A. Ghosh, K. S. Sugi, A. Nag, E. Khatun, B. Varghese, G. Paramasivam, S. Antharjanam, G. Natarajan and T. Pradeep, *Angew. Chem., Int. Ed.*, 2019, **58**, 189–194.
- H. Yang, Y. Wang, H. Huang, L. Gell, L. Lehtovaara, S. Malola, H. Häkkinen and N. Zheng, *Nat. Commun.*, 2013, **4**, 1–8.
- W. Fei, S. Antonello, T. Dainese, A. Dolmella, M. Lahtinen, K. Rissanen, A. Venzo and F. Maran, *J. Am. Chem. Soc.*, 2019, **141**, 16033–16045.
- J. Q. Wang, S. Shi, R. L. He, S. F. Yuan, G. Y. Yang, G. J. Liang and Q. M. Wang, *J. Am. Chem. Soc.*, 2020, **142**, 18086–18092.
- N. Yan, N. Xia, L. Liao, M. Zhu, F. Jin, R. Jin and Z. Wu, *Sci. Adv.*, 2018, **4**, 7259–7271.
- W. Jiang, Y. Bai, Q. Li, X. Yao, H. Zhang, Y. Song, X. Meng, H. Yu and M. Zhu, *Inorg. Chem.*, 2020, **59**, 5394–5404.
- V. R. Jupally, A. C. Dharmaratne, D. Crasto, A. J. Huckaba, C. Kumara, P. R. Nimmala, N. Kothalawala, J. H. Delcamp and A. Dass, *Chem. Commun.*, 2014, **50**, 9895–9898.
- C. A. Fields-Zinna, J. S. Sampson, M. C. Crowe, J. B. Tracy, J. F. Parker, A. M. deNey, D. C. Muddiman and R. W. Murray, *J. Am. Chem. Soc.*, 2009, **131**, 13844–13851.
- L. A. Angel, L. T. Majors, A. C. Dharmaratne and A. Dass, *ACS Nano*, 2010, **4**, 4691–4700.
- Y. Zeng, S. Havenridge, M. Gharib, A. Baksi, K. L. D. M. Weerawardene, A. R. Ziefuß, C. Strelow, C. Rehbock, A. Mews, S. Barcikowski, M. M. Kappes, W. J. Parak, C. M. Aikens and I. Chakraborty, *J. Am. Chem. Soc.*, 2021, **143**, 9405–9414.
- S. Chen, W.-H. H. Fang, L. Zhang and J. Zhang, *Angew. Chem., Int. Ed.*, 2018, **57**, 11252–11256.
- C. P. Joshi, M. S. Bootharaju, M. J. Alhilaly and O. M. Bakr, *J. Am. Chem. Soc.*, 2015, **137**, 11578–11581.
- A. Mathew, G. Natarajan, L. Lehtovaara, H. Hä, R. M. Kumar, V. Subramanian, A. Jaleel and T. Pradeep, *ACS Nano*, 2014, **8**, 139–152.
- A. Sagadevan, A. Ghosh, P. Maity, O. F. Mohammed, O. M. Bakr and M. Rueping, *J. Am. Chem. Soc.*, 2022, **144**, 12052–12061.
- M. Daté, H. Imai, S. Tsubota and M. Haruta, *Catal. Today*, 2007, **122**, 222–225.
- J. V. Rival, P. Mymoona, K. M. Lakshmi, Nonappa, T. Pradeep and E. S. Shibu, *Small*, 2021, **17**, 2005718.
- J. Ahmed, P. Trinh, A. M. Mugweru and A. K. Ganguli, *Solid State Sci.*, 2011, **13**, 855–861.
- A. K. Das, S. Mukherjee, S. R. Sreehari, A. S. Nair, S. Bhandary, D. Chopra, D. Sanyal, B. Pathak and S. Mandal, *ACS Nano*, 2020, **14**, 16681–16688.
- A. Nag, P. Chakraborty, M. Bodiuzzaman, T. Ahuja, S. Antharjanam and T. Pradeep, *Nanoscale*, 2018, **10**, 9851–9855.
- Z. Wu, J. Liu, Y. Gao, H. Liu, T. Li, H. Zou, Z. Wang, K. Zhang, Y. Wang, H. Zhang and B. Yang, *J. Am. Chem. Soc.*, 2015, **137**, 12906–12913.
- R. Kazan, B. Zhang and T. Bürgi, *Dalton Trans.*, 2017, **46**, 7708–7713.
- M. A. H. Muhammed, P. K. Verma, S. K. Pal, A. Retnakumari, M. Koyakutty, S. Nair and T. Pradeep, *Chem. – Eur. J.*, 2010, **16**, 10103–10112.
- E. S. Shibu, M. A. H. Muhammed, T. Tsukuda and T. Pradeep, *J. Phys. Chem. C*, 2008, **112**, 12168–12176.
- P. L. Xavier, K. Chaudhari, P. K. Verma, S. K. Pal and T. Pradeep, *Nanoscale*, 2010, **2**, 2769–2776.
- Y. Chen, M. Zhou, Q. Li, H. Gronlund and R. Jin, *Chem. Sci.*, 2020, **11**, 8176–8183.
- S. Maity, D. Bain and A. Patra, *J. Phys. Chem. C*, 2019, **123**, 2506–2515.
- Q. Yao, Z. Wu, Z. Liu, Y. Lin, X. Yuan and J. Xie, *Chem. Sci.*, 2021, **12**, 99–127.
- G. N. Parsons and R. D. Clark, *Chem. Mater.*, 2020, **32**, 4920–4953.
- M. H. Naveen, R. Khan and J. H. Bang, *Chem. Mater.*, 2021, **33**, 7595–7612.
- S. Hossain, Y. Niihori, L. V. Nair, B. Kumar, W. Kurashige and Y. Negishi, *Acc. Chem. Res.*, 2018, **51**, 3114–3124.
- Y. Song, Y. Li, M. Zhou, X. Liu, H. Li, H. Wang, Y. Shen, M. Zhu and R. Jin, *Sci. Adv.*, 2021, **7**, eabd2091.

- 38 S. Wang, Y. Song, S. Jin, X. Liu, J. Zhang, Y. Pei, X. Meng, M. Chen, P. Li and M. Zhu, *J. Am. Chem. Soc.*, 2015, **137**, 4018–4021.
- 39 L. Wang, K. Shen, M. Chen and Y. Zhu, *Nanoscale*, 2019, **11**, 13767–13772.
- 40 E. Khatun, P. Chakraborty, B. R. Jacob, G. Paramasivam, M. Bodiuzzaman, A. Dar and T. Pradeep, *Chem. Mater.*, 2020, **32**(1), 611–619.
- 41 E. Khatun and T. Pradeep, *ACS Omega*, 2021, **6**, 1–16.
- 42 S. Knoppe and T. Bürgi, *Phys. Chem. Chem. Phys.*, 2013, **15**, 15816–15820.
- 43 Z. Huang, Y. Ishida, K. Narita and T. Yonezawa, *J. Phys. Chem. C*, 2018, **122**, 18142–18150.
- 44 S. Knoppe, A. C. Dharmaratne, E. Schreiner, A. Dass and T. Bürgi, *J. Am. Chem. Soc.*, 2010, **132**, 16783–16789.
- 45 Y. Niihori, S. Hossain, B. Kumar, L. V. Nair, W. Kurashige and Y. Negishi, *APL Mater.*, 2017, **5**, 053201.
- 46 S. Wang, L. Xiong, G. Sun, L. Tang, J. Zhang, Y. Pei and M. Zhu, *Nanoscale Adv.*, 2020, **2**, 664–668.
- 47 B. Zhang, O. V. Safonova, S. Pollitt, G. Salassa, A. Sels, R. Kazan, Y. Wang, G. Rupperecht, N. Barrabés and T. Bürgi, *Phys. Chem. Chem. Phys.*, 2018, **20**, 5312–5318.
- 48 K. R. Krishnadas, A. Ghosh, A. Baksi, I. Chakraborty, G. Natarajan and T. Pradeep, *J. Am. Chem. Soc.*, 2016, **138**, 140–148.
- 49 K. R. Krishnadas, A. Baksi, A. Ghosh, G. Natarajan and T. Pradeep, *Nat. Commun.*, 2016, **7**, 1–9.
- 50 M. Neumaier, A. Baksi, P. Weis, E. K. Schneider, P. Chakraborty, H. Hahn, T. Pradeep and M. M. Kappes, *J. Am. Chem. Soc.*, 2021, **143**, 6969–6980.
- 51 R. Kazan, U. Müller and T. Bürgi, *Nanoscale*, 2019, **11**, 2938–2945.
- 52 P. Chakraborty, A. Nag, G. Natarajan, N. Bandyopadhyay, G. Paramasivam, M. K. Panwar, M. Kumar Panwar, J. Chakrabarti and T. Pradeep, *Sci. Adv.*, 2019, **5**, eaau7555.
- 53 Nonappa, T. Lahtinen, J. S. Haataja, T. R. Tero, H. Häkkinen and O. Ikkala, *Angew. Chem., Int. Ed.*, 2016, **55**, 16035–16038.
- 54 A. Som, A. Griffio, I. Chakraborty, H. Hähl, B. Mondal, A. Chakraborty, K. Jacobs, P. Laaksonen, O. Ikkala, T. Pradeep, A. Som, O. Ikkala, A. Griffio, P. Laaksonen, H. Hähl, K. Jacobs, I. Chakraborty, B. Mondal, A. Chakraborty and T. Pradeep, *Small*, 2022, **18**, 2201707.
- 55 Y. Zhou and H. C. Zeng, *Small*, 2016, **12**, 2652–2664.
- 56 A. Dong, J. Chen, P. M. Vora, J. M. Kikkawa and C. B. Murray, *Nature*, 2010, **466**, 474–477.
- 57 A. Som, A. Griffio, I. Chakraborty, H. Hähl, B. Mondal, A. Chakraborty, K. Jacobs, P. Laaksonen, O. Ikkala, T. Pradeep, A. Som, O. Ikkala, A. Griffio, P. Laaksonen, H. Hähl, K. Jacobs, I. Chakraborty, B. Mondal, A. Chakraborty and T. Pradeep, *Small*, 2022, **18**, 2201707.
- 58 J. Pang, S. Xiong, F. Jaeckel, Z. Sun, D. Dunphy and C. J. Brinker, *J. Am. Chem. Soc.*, 2008, **130**, 3284–3285.
- 59 A. Baksi, P. Chakraborty, S. Bhat, G. Natarajan and T. Pradeep, *Chem. Commun.*, 2016, **52**, 8397–8400.
- 60 X. Kang, H. Chong and M. Zhu, *Nanoscale*, 2018, **10**, 10758–10834.
- 61 J. Naktiyok and A. K. Özer, *Niğde Ömer Halisdemir Üniversitesi Mühendislik Bilimleri Dergisi*, 2019, **8**(2), 1292–1298, DOI: [10.28948/ngumuh.598177](https://doi.org/10.28948/ngumuh.598177).
- 62 J. Wei, H. Wang, Y. Deng, Z. Sun, L. Shi, B. Tu, M. Luqman and D. Zhao, *J. Am. Chem. Soc.*, 2011, **133**, 20369–20377.
- 63 J. A. Kephart, C. G. Romero, C. C. Tseng, K. J. Anderton, M. Yankowitz, W. Kaminsky and A. Velian, *Chem. Sci.*, 2020, **11**, 10744–10751.
- 64 O. P. Keabadile, A. O. Aremu, S. E. Elugoke and O. E. Fayemi, *Nanomaterials*, 2020, **10**, 2502–2520.
- 65 Y. R. Luo, *Compr. Handb. Chem. Bond Energies*, 2007, pp. 1–1656.
- 66 Y. Negishi, K. Munakata, W. Ohgake and K. Nobusada, *J. Phys. Chem. Lett.*, 2012, **3**, 2209–2214.
- 67 G. Natarajan, A. Mathew, Y. Negishi, R. L. Whetten and T. Pradeep, *J. Phys. Chem. C*, 2015, **119**, 27768–27785.
- 68 S. Bhat, R. P. Narayanan, A. Baksi, P. Chakraborty, G. Paramasivam, R. Rajan, J. Methikkalam, A. Nag, G. Natarajan and T. Pradeep, *J. Phys. Chem. C*, 2018, **122**(34), 19455–19462.
- 69 Nonappa and O. Ikkala, *Adv. Funct. Mater.*, 2018, **28**, 1704328.
- 70 A. Chakraborty, A. C. Fernandez, A. Som, B. Mondal, G. Natarajan, G. Paramasivam, T. Lahtinen, H. Häkkinen, Nonappa and T. Pradeep, *Angew. Chem., Int. Ed.*, 2018, **57**, 6522–6526.
- 71 P. Bose, P. Chakraborty, J. S. Mohanty, Nonappa, A. Ray Chowdhuri, E. Khatun, T. Ahuja, A. Mahendranath and T. Pradeep, *Nanoscale*, 2020, **12**, 22116–22128.